nature cell biology

CDK1-dependent phosphorylation of EZH2 suppresses methylation of H3K27 and promotes osteogenic differentiation of human mesenchymal stem cells

Yongkun Wei[1], Ya-Huey Chen[2], Long-Yuan Li[2,3,4,9], Jingyu Lang[1], Su-Peng Yeh[5], Bin Shi[1], Cheng-Chieh Yang[1], Jer-Yen Yang[1], Chun-Yi Lin[2], Chien-Chen Lai[6,7] and Mien-Chie Hung[1,2,3,4,8,9]

Enhancer of zeste homologue 2 (EZH2) is the catalytic subunit of Polycomb repressive complex 2 (PRC2) and catalyses the trimethylation of histone H3 on Lys 27 (H3K27), which represses gene transcription. EZH2 enhances cancer-cell invasiveness and regulates stem cell differentiation. Here, we demonstrate that EZH2 can be phosphorylated at Thr 487 through activation of cyclin-dependent kinase 1 (CDK1). The phosphorylation of EZH2 at Thr 487 disrupted EZH2 binding with the other PRC2 components SUZ12 and EED, and thereby inhibited EZH2 methyltransferase activity, resulting in inhibition of cancer-cell invasion. In human mesenchymal stem cells, activation of CDK1 promoted mesenchymal stem cell differentiation into osteoblasts through phosphorylation of EZH2 at Thr 487. These findings define a signalling link between CDK1 and EZH2 that may have an important role in diverse biological processes, including cancer-cell invasion and osteogenic differentiation of mesenchymal stem cells.

The Polycomb group (PcG) protein EZH2 is a histone lysine methyltransferase associated with transcriptional repression. EZH2 functions in the multi-protein complex PRC2, which includes SUZ12 (suppressor of zeste 12) and EED (embryonic ectoderm development)[1,2]. EZH2 catalyses the addition of methyl groups to histone H3 at Lys 27 (H3K27) in target gene promoters, leading to epigenetic silencing. EZH2 has an important role in controlling biological processes including X-chromosome inactivation, germline development, stem cell pluripotency and cancer metastasis[3].

EZH2 is aberrantly overexpressed in aggressive solid tumours and overexpression of EZH2 has been implicated in cancer progression and metastases[4–7]. In addition, *EZH2* knockdown leads to decreased proliferation of cancer cells and a delay in the G2/M transition of the cell cycle[8]. As EZH2 has a role in the G2/M transition and CDK1 is one of the major G2/M kinases, and because both have a central function in controlling self-renewal and lineage specification of stem cells[9], we investigated whether EZH2 is regulated by CDK1.

First, we investigated whether alteration of CDK1 activity affects H3K27 trimethylation. H3K27 trimethylation was increased in several cancer-cell lines after treatment with a CDK1 inhibitor, CGP74514A[10], at a concentration (2 μM) that is specific to CDK1 in these lines (Fig. 1a). The activity of CDK1 was inhibited by CGP74514A, as assessed by *in vitro* kinase assay of CDK1 using histone H1 as a substrate (Fig. 1a, bottom). There was no change in EZH2, SUZ12 and EED protein level. In addition, H3K27 trimethylation level increased in accordance with CGP74514A in a dose- and time-dependent manner (Supplementary Information, Fig. S1a, b). Similar results were found when cells were treated with Roscovitine, a pan-CDK inhibitor (data not shown). Consistently, knockdown of endogenous *CDK1* expression by two different shRNA (to exclude potential off-target effects of the shRNA), or by small interfering RNA (siRNA), enhanced H3K27 trimethylation (Fig. 1b and Supplementary Information, Fig. S1c). In addition, expression of a dominant-negative mutant CDK1 (DN-CDK1; ref. 11) also increased H3K27 trimethylation (Fig. 1c). As we had found that H3K27 trimethylation is increased with inhibition of CDK1 we next examined whether inhibition of CDK1 activity affects the expression of known EZH2-target genes. We tested gene expression of the *HOXA* family members using quantitative reverse transcription polymerase chain reaction (qRT–PCR). We found that expression of *HOXA* genes was suppressed by treatment with CGP74514A (Fig. 1d), indicating that inhibition of CDK1 affects the expression of EZH2-target genes.

As inactivation of CDK1 enhances trimethylation of H3K27, resulting in downregulation of EZH2-targeted gene expression, we next investigated whether CDK1, a serine/threonine kinase, might inhibit histone

[1]Department of Molecular and Cellular Oncology, The University of Texas M.D. Anderson Cancer Center, Houston, TX 77030, USA. [2]Center for Molecular Medicine, China Medical University Hospital, Taichung 404, Taiwan. [3]Graduate Institute of Cancer Biology, China Medical University, Taichung 404, Taiwan. [4]Asia University, Taichung 413, Taiwan. [5]Division of Hematology and Oncology, Department of Medicine, China Medical University and Hospital, Taichung 404, Taiwan. [6]Graduate Institute of Chinese Medical Science, China Medical University, Taichung 404, Taiwan. [7]Institute of Molecular Biology, National Chung Hsing University, Taichung 402, Taiwan. [8]Program in Cancer Biology, The University of Texas Graduate School of Biomedical Sciences at Houston, Houston, TX 77030, USA.
[9]Correspondence should be addressed to L.-Y.L. or M.-C.H. (e-mail: lyl@mail.cmu.edu.tw or mhung@mdanderson.org)

Received 10 June 2010; accepted 10 November 2010; published online 05 December 2010; DOI: 10.1038/ncb2139

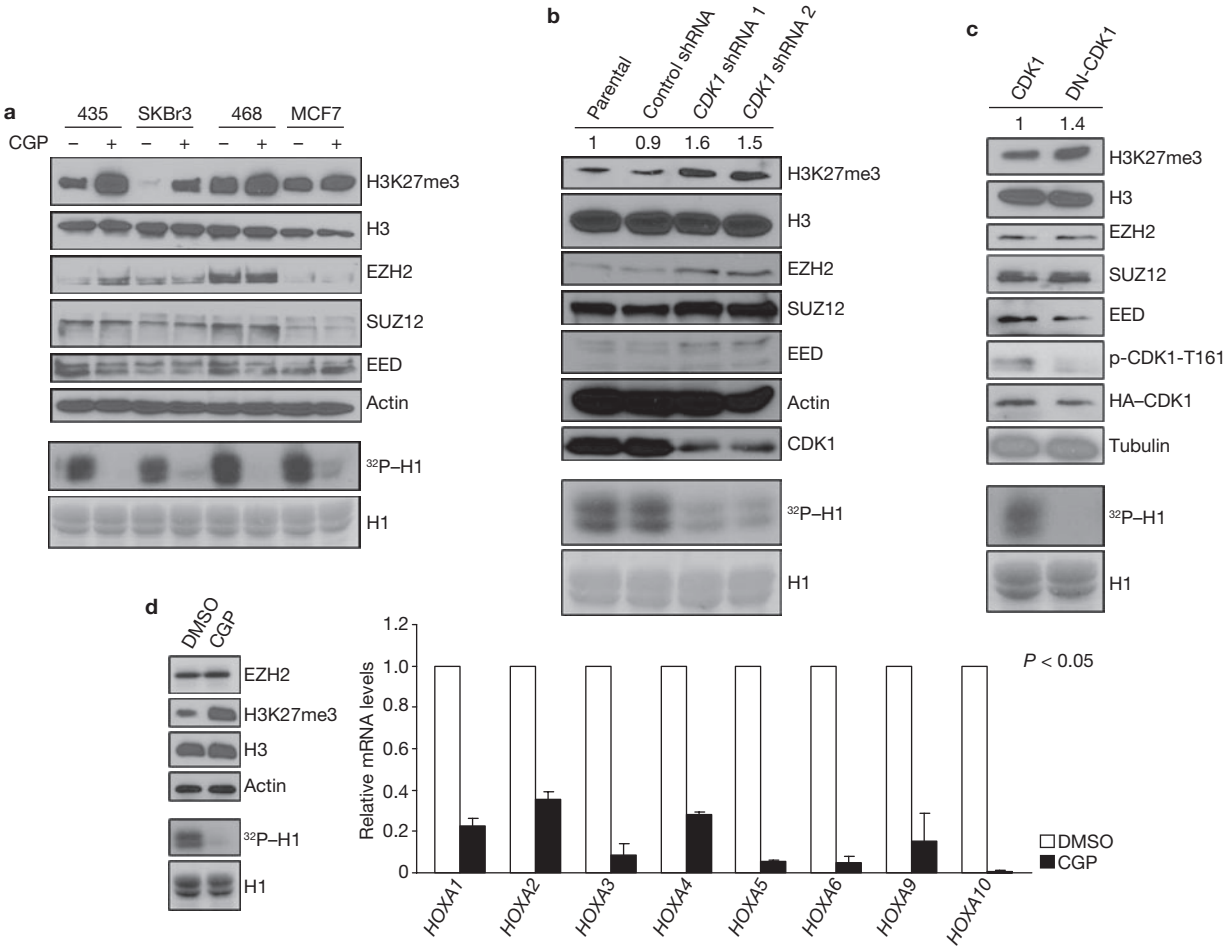

Figure 1 CDK1 negatively regulates H3K27 trimethylation. (**a**) Top: 435, SKBr3, 468 and MCF7 cells were treated with CGP74514A as indicated, and the lysates were analysed by immunoblot using antibodies against the specified proteins. Bottom: *in vitro* kinase assay. CDK1, immunoprecipitated from the cell lines treated with CGP74514A as indicated at the top, was incubated with H1 and [γ-^{32}P]ATP. Reaction products were resolved by SDS–PAGE and visualized by autoradiography (equal loading of H1 was assessed by Coomassie-stained gel shown at the bottom). (**b**) Lysates from MCF7 cells infected with lentiviruses expressing control or two different *CDK1* shRNA were immunoblotted with antibodies against the indicated proteins. Relative intensities of the H3K27me3 bands are shown, normalized to the H3K27me3 band from parental MCF7 cells. Bottom: *in vitro* kinase assay, performed as in **a**, with CDK1 immunoprecipitated from cells treated as indicated at the top. (**c**) Lysates of 293T cells transfected with plasmids encoding cyclin B, and CDK1 or dominant-negative mutant CDK1 (DN-CDK1) were immunoblotted with antibodies against the indicated proteins. Relative intensities of the H3K27me3 bands are shown, normalized to the H3K27me3 band from 293T cells transfected with plasmid encoding CDK1. p-CDK1-T161; CDK1 phosphorylated at Thr 161. Bottom: *in vitro* kinase assay, performed as in **a**, with CDK1 immunoprecipitated from cells transfected as indicated at the top. (**d**) Left top: immunoblot of lysate from HEK293 cells treated with DMSO or CGP using antibodies against the indicated proteins. Left bottom: *in vitro* kinase assay, performed as in **a**, with CDK1 immunoprecipitated from cells treated as indicated at the top. Right: analysis of mRNA levels of *HOXA* families by qRT–PCR after treatment of HEK293 cells with DMSO or CGP74514A. Data are means ± s.e.m. ($n = 3$). Uncropped images of blots are shown in Supplementary Information, Fig. S6.

methyltransferase (HMTase) activity of EZH2 through phosphorylation of EZH2. We first examined whether CDK1 physically interacts with EZH2 by a co-immunoprecipitation experiment, which demonstrated an association between Myc-tagged EZH2 and haemmagglutinin (HA)-tagged CDK1 (Fig. 2a). We further validated the interaction using a GST pulldown assay to demonstrate that CDK1 binds to EZH2 (Fig. 2b). Importantly, this association was also detected with endogenous CDK1 and EZH2 by reciprocal immunoprecipitation, indicating that these two molecules interact *in vivo* (Fig. 2c).

Next, we investigated whether CDK1 is able to phosphorylate EZH2. An *in vitro* kinase assay demonstrated that CDK1 catalysed the phosphorylation of EZH2, but not glutathione *S*-transferase (GST; data not shown). Mass spectrometry analysis was used to identify which residue in EZH2 is phosphorylated. We found that Thr 487 of EZH2 was phosphorylated both *in vivo* (Supplementary Information, Fig. S2a), and *in vitro* by CDK1 (Fig. 2d). When we replaced the Thr 487 residue with alanine (EZH2^{T487A}), CDK1 was no longer able to phosphorylate the mutant EZH2, as assessed by *in vitro* CDK1 kinase assay (Fig. 2e). In cell culture, inhibition of CDK1 with CGP74514A also reduced the phosphorylation of wild-type EZH2 (Fig. 2f; lanes 2 and 3) and again, the phosphorylation level of EZH2^{T487A} mutant was virtually undetectable in an immunoblot using antibody against phosphorylated serine/threonine (Fig. 2f; lanes 4 versus 2). We also compared the phosphorylation level of wild-type EZH2 and EZH2^{T487A} by *in vivo* ^{32}P-labelling experiments. Phosphorylation of wild-type EZH2 occurred *in vivo*, but was inhibited by expression of *CDK1* shRNA (Fig. 2g). The phosphorylation

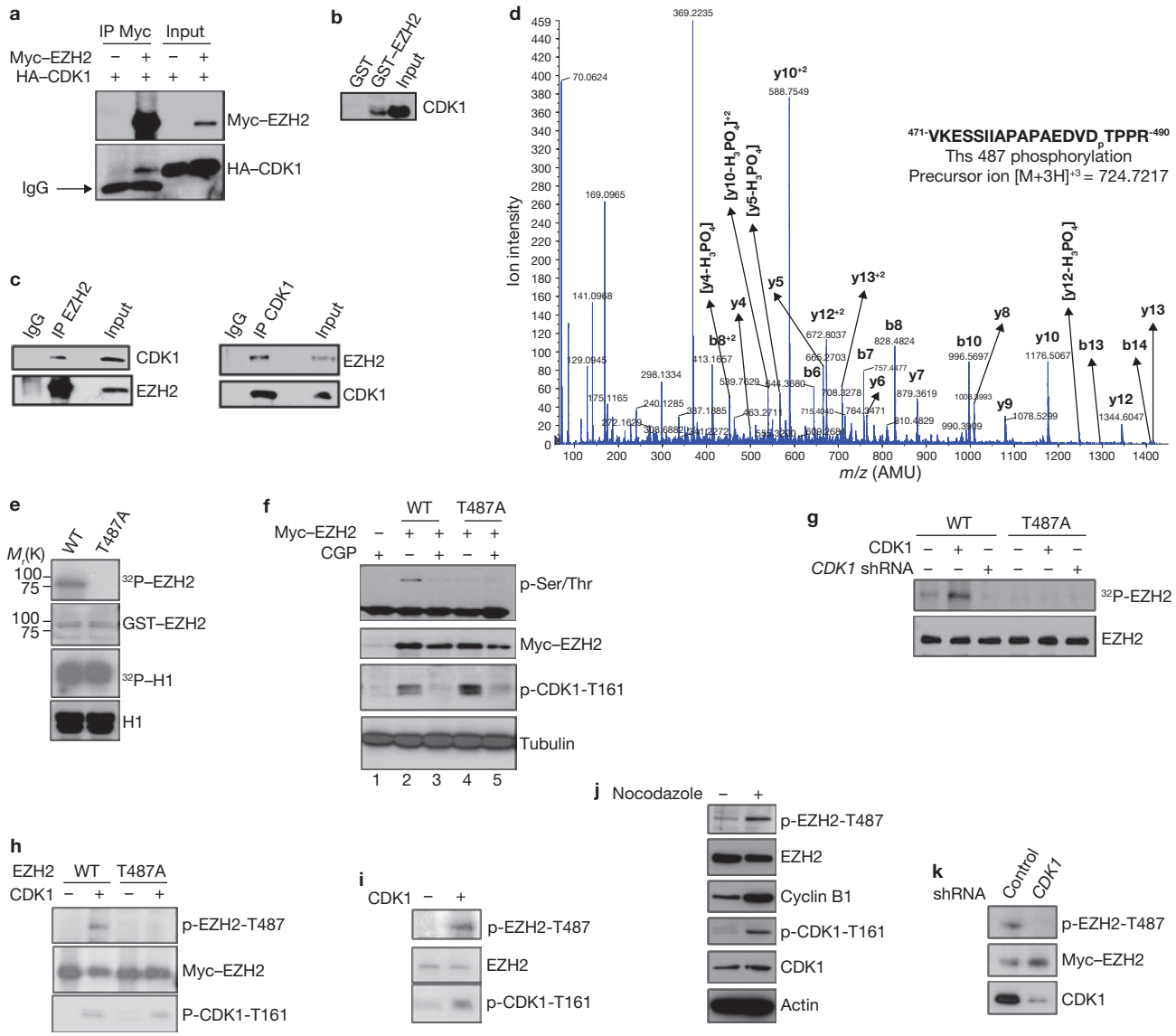

Figure 2 CDK1 interacts with, and phosphorylates, EZH2 at Thr 487. (**a**) Lysates from 293T cells, transfected with plasmids encoding Myc–EZH2 and HA–CDK1 as indicated, were immunoprecipitated (IP) using anti-Myc and analysed by immunoblot using anti-Myc or anti-HA. IgG; immunoglobulin G. (**b**) Pulldowns. GST and GST–EZH2 were incubated with lysate from HeLa cells. Bound CDK1 was detected by immunoblotting. (**c**) Lysate from MCF7 cells was immunoprecipitated with antibodies against EZH2 (left) or CDK1 (right), and analysed by immunoblotting. (**d**) Cyclin B, CDK1 and GST–EZH2 were subjected to an *in vitro* kinase assay and analysed by mass spectrometry. The spectrum of the charged ion (*m/z* 724.7217) shows that Thr 487 is phosphorylated (lower case p) in the indicated peptide (top right). b ions, fragmentation ions containing the amino terminus of the peptide; y ions, fragmentation ions containing the carboxy terminus of the peptide. (**e**) *In vitro* kinase assay with CDK1, cyclin B, and wild-type GST–EZH2 (WT) or GST– EZH2^{T487A}. Phosphorylation of EZH2 and H1 was visualized by autoradiography, and loading of GST–EZH2 and H1 was assessed by Coomassie-stained gel. (**f**) 293T cells were transfected with plasmids encoding wild-type Myc–EZH2 or Myc–EZH2^{T487A} and treated with CDK1 inhibitor CGP74514A or DMSO. Lysates were immunoprecipitated with anti-Myc and analysed by immunoblotting. (**g**) MCF7 cells stably expressing wild-type Myc–EZH2 or Myc–EZH2^{T487A} were transfected with control vector or plasmids encoding CDK1 and cyclin B, and infected with lentivirus expressing *CDK1* shRNA, as indicated. Cells were labelled with [^{32}P]-orthophosphate, EZH2 was immunoprecipitated from lysates with anti-Myc and analysed by autoradiography. Immunoblotting was used to confirm equal loading of EZH2 (bottom). (**h**) HeLa cells expressing Myc–EZH2 or Myc–EZH2^{T487A} were transfected with plasmid encoding CDK1 and cyclin B, or control vector. Cell lysates were immunoprecipitated with anti-Myc and immunoblotted. (**i**) Lysates of HeLa cells transfected with plasmid encoding CDK1 and cyclin B, or control vector, were immunoprecipitated with anti-EZH2, and immunoblotted. (**j**) Immunoblot of lysates from HeLa cells treated with Nocodazole as indicated. Cell lysates were immunoprecipitated with anti-EZH2. (**k**) MCF7 cells stably expressing wild-type Myc–EZH2 were infected with lentivirus expressing control or *CDK1* shRNA. Cell lysates were immunoprecipitated with anti-Myc and immunoblotted. Uncropped images of blots are shown in Supplementary Information, Fig. S6.

level of EZH2^{T487A} was much lower than that of wild-type EZH2 and was not altered by expression of *CDK1* shRNA (Fig. 2g). These results suggested that Thr 487 is a major phosphorylation site of EZH2 *in vivo* and can be activated by CDK1.

To confirm that CDK1 does indeed phosphorylate EZH2 at Thr 487 *in vivo*, we generated an antibody that specifically recognizes EZH2 phosphorylated at Thr 487, but fails to detect an unphosphorylated EZH2 peptide (Supplementary Information, Fig. S2b). To confirm the specificity of

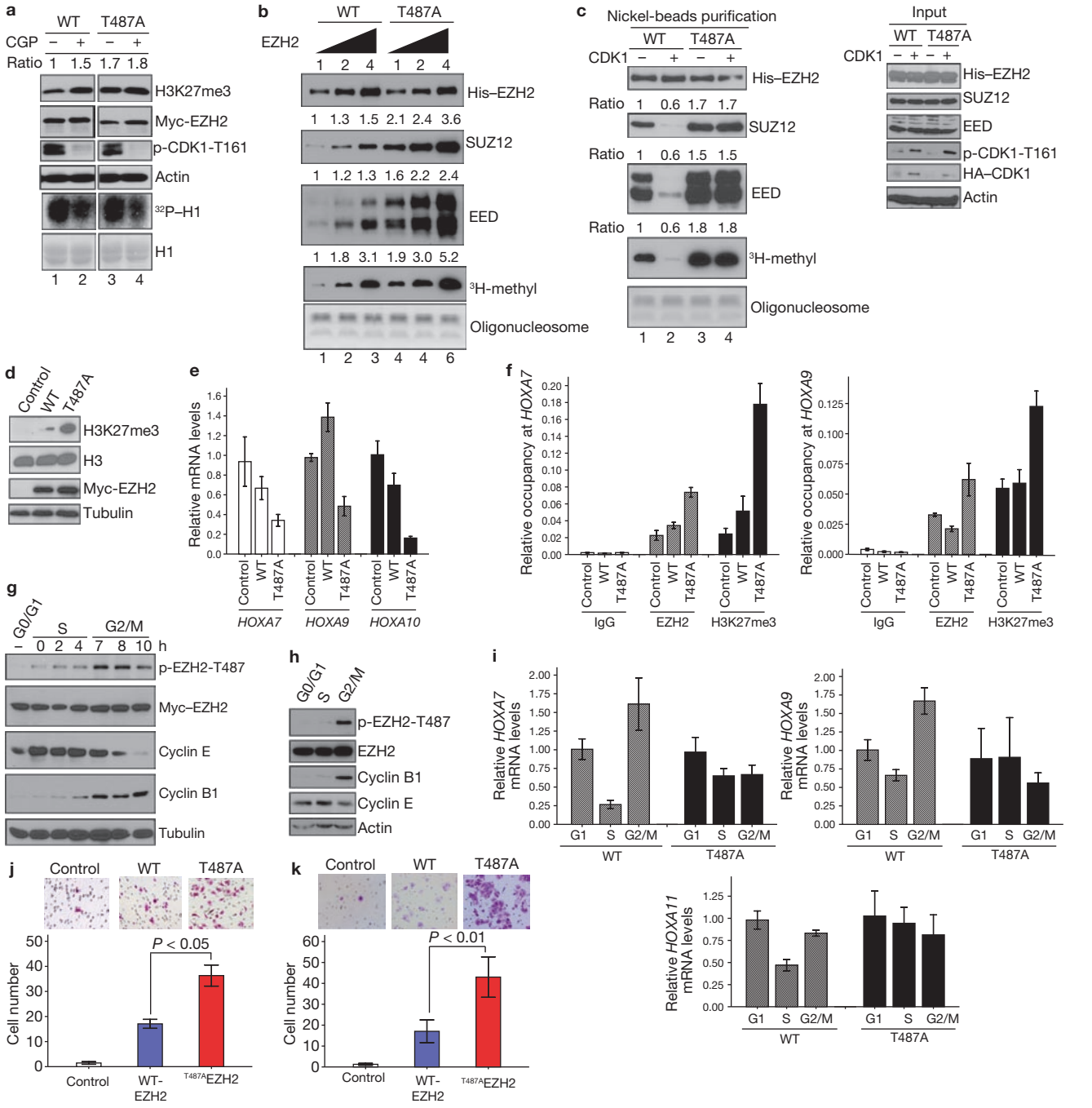

Figure 3 CDK1-mediated phosphorylation of EZH2 promotes disassociation of EZH2 from SUZ12 and EED and suppresses EZH2 HMTase activity. (**a**) HeLa cells were transfected with plasmids encoding wild-type EZH2 or EZH2^{T487A} and treated with CGP74514A as indicated. Top: immunoblot. Relative intensity of the H3K27me3 bands is indicated. Bottom: Autoradiograph and immunoblot of *in vitro* kinase assay using H1 as substrate. (**b**) *In vitro* histone methyltransferase assay. PRC2 complexes were purified from MCF7 cell lines stably expressing wild-type Myc-His–EZH2 or Myc-His–EZH2^{T487A} and 0.5, 1 and 2 μg were used in the assay. Top: immunoblots of purified proteins. Bottom: proteins were incubated with oligonucleosome and ^{3}H-labelled *S*-adenosylmethionine. Methylation was assessed by autoradiography and oligonucleosome loading by Coomassie-stained gel. Relative intensities of bands are indicated at the top of each panel. (**c**) MCF7 cell lines as in **b** were transfected with control vector or plasmids encoding HA–CDK1. Left: immunoblots of experiment performed as in **b**. Right: immunoblot of lysates from MCF7 cells used in protein purification. (**d**) Immunoblot of lysates from stable MCF7 transfectants, established by transfection of cells with control vector or plasmids encoding Myc–EZH2 or Myc–EZH2^{T487A}. (**e**) qRT–PCR of *HOXA* genes in MCF7 cell lines described in **d**. Data are means ± s.d. from three individual experiments. (**f**) Quantitative chromatin immunoprecipitation analysis on *HOXA7* and *HOXA9* promoters in MCF7 cell lines as described in **d**. Data are means ± s.d. from three individual experiments. (**g**) Immunoblot of MCF7 cell lines stably expressing wild-type EZH2, treated by serum starvation (to collect cells at G0/G1 phase) or by double thymidine blockage and release (to collect cells at S and G2/M phases). (**h**) Immunoblot of HeLa cells treated as in **g**. (**i**) qRT–PCR of *HOXA* gene expression in MCF7 stable cell lines treated as in **g**. Data are means ± s.d. from three individual experiments. (**j**) Images and quantification of cell migration of MCF7 stable cell lines. Data are means ± s.e.m. from three individual experiments. (**k**) Images and quantification of cell invasion of MCF7 stable cell lines. Data are means ± s.e.m. from three individual experiments. Uncropped images of blots are shown in Supplementary Information, Fig. S6.

the antibody, it was incubated with wild-type Myc–EZH2 or non-phosphorylatable Myc–EZH2^{T487A}, which were resolved on a SDS–PAGE gel and immunoblotted. The signal from the phospho-EZH2-Thr 487 antibody alone was lowered when incubated with phosphorylated peptide, but not unphosphorylated petide (Supplementary Information, Fig. S2c). Using the phospho-EZH2-Thr 487 antibody, we immunoblotted lysates from HeLa cells co-transfected with plasmids encoding CDK1 and EZH2 or EZH2^{T487A}, which demonstrated that CDK1 stimulated the Thr 487 phosphorylation of wild-type EZH2, but not EZH2^{T487A} (Fig. 2h). The endogenous level of phosphorylated EZH2 at Thr 487 was also increased when CDK1 was overexpressed (Fig. 2i). Activation of CDK1 by treatment of cells with Nocodazole, which arrests cells in G2/M phase, can also induce endogenous EZH2 phosphorylation at Thr 487 (Fig. 2j). Furthermore, depletion of endogenous *CDK1* by transduction of cells with *CDK1* shRNA reduced EZH2 phosphorylation (Fig. 2k), suggesting that endogenous CDK1 is required for EZH2 phosphorylation at Thr 487. These data indicate that EZH2 is phosphorylated at Thr 487 by CDK1 both *in vitro* and *in vivo*.

Next, we investigated whether EZH2 phosphorylation mediates the ability of CDK1 to inhibit H3K27 trimethylation. Consistently, we observed that the H3K27 trimethylation level was higher in HeLa cells transfected with plasmids encoding the mutant EZH2^{T487A} than in cells transfected with plasmids encoding wild-type EZH2 (Fig. 3a; lanes 1 and 3). Additionally, inhibition of CDK1 with CGP74514A enhanced H3K27 trimethylation in cells transfected with plasmids encoding wild-type EZH2, but not in cells transfected with plasmids encoding EZH2^{T487A} (Fig. 3a; lanes 1–4 of Fig. 3a are from the same gel). Together, these results suggest that phosphorylation of EZH2 at Thr 487 by CDK1 leads to a decrease in H3K27 trimethylation.

As CDK1 suppression of H3K27 trimethylation is mediated by EZH2, we investigated whether phosphorylation of EZH2 by CDK1 alters the HMTase activity of EZH2. An *in vitro* HMTase activity assay with oligonucleosome as the substrate showed that the EZH2^{T487A} mutant exhibited higher HMTase activity than that of wild-type EZH2 (Fig. 3b bottom, lanes 4–6 versus lanes 1–3; Fig. 3c, lane 3 versus 1). Activation of CDK1 by co-transfection of plasmids expressing cyclin B and CDK1 inhibited HMTase activity of wild-type EZH2 (Fig. 3c; lane 2 versus 1), but not EZH2^{T487A} (Fig. 3c; lane 4 versus 3). In addition, cells stably expressing EZH2^{T487A} also exhibited higher H3K27 trimethylation than that of wild-type EZH2 (Fig. 3d). Together, these results suggest that phosphorylation of EZH2 at Thr 487 by CDK1 inhibits HMTase activity of EZH2.

EZH2 forms a complex with SUZ12 and EED (PRC2) *in vivo*[1,2] and a stable complex is required for its HMTase activity. As CDK1-mediated EZH2 phosphorylation did not change the protein level of EZH2, but inhibited its HMTase activity, we next investigated whether phosphorylation might interrupt the interaction of EZH2 with SUZ12 and EED. We examined the interaction of EZH2 with SUZ12 and EED through purification of Myc-His-tagged EZH2 complex from cell lines stably expressing wild-type EZH2 and EZH2^{T487A}. There was stronger binding between SUZ12, EED and EZH2^{T487A} when compared with wild-type EZH2 (Fig. 3b; lanes 4–6 versus lanes 1–3 and Supplementary Information, Fig. S3a and Fig. 3c; lanes 3 versus 1). Activation of CDK1 led to the inhibition of wild-type EZH2 binding to SUZ12 and EED (Fig. 3c; lane 2 versus 1), but did not affect the binding of EZH2^{T487A} (Fig. 3c; lane 4 versus 3). These data support the hypothesis that phosphorylation of EZH2 by CDK1 inhibits its HMTase activity through disruption of the binding between EZH2 and SUZ12 and EED.

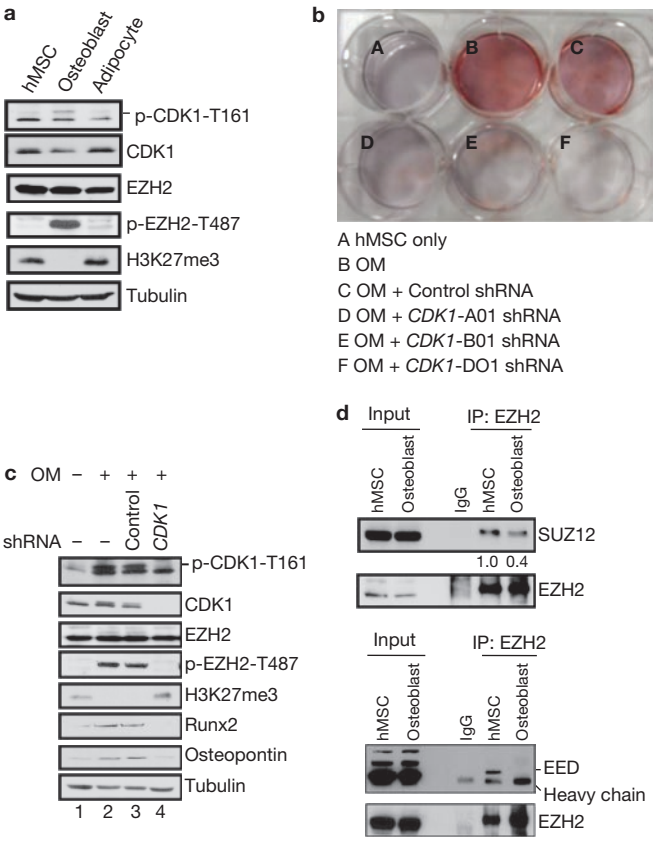

Figure 4 Phosphorylation of EZH2 by CDK1 promotes osteogenic differentiation of human mesenchymal stem cells. (**a**) Osteoblast differentiation medium induces activation of CDK1 in hMSCs. Immunoblot of lysates from undifferentiated cells or cells differentiated into osteoblasts or adipocytes. (**b**) hMSCs were left untreated or were treated with osteoblast differentiation medium (OM) and shRNA as indicated. Alizarin Red S staining was performed at day 7. Differentiated stem cells positive for Alizarin Red S are stained red. (**c**) Effect of *CDK1* knockdown on the expression of osteogenic-specific genes in hMSCs. Cells were cultured in control medium or osteoblast differentiation medium, and infected with lentiviruses expressing control or *CDK1* shRNA as indicated. Cell lysates were subjected to immunoblot analysis. (**d**) Disruption of PRC2 complex after osteogenic differentiation. Lysates from cells undifferentiated or differentiated into osteoblasts were immunoprecipitated with EZH2 antibody and subjected to immunoblot analysis as indicated.

To examine whether EZH2 phosphorylation mediated by CDK1 affects its transcriptional repressor function, we analysed expression levels of EZH2-target *HOXA* genes using qRT–PCR. We found that a number of genes in *HOXA* clusters are repressed by expression of EZH2^{T487A} (Fig. 3e). Consistent with these results, we found that there was high EZH2 and H3K27 trimethylation on the *HOXA7* and *HOXA9* promoters, as detected by a quantitative chromatin immunoprecipitation (qChIP) assay (Fig. 3f). These results suggest that phosphorylation of EZH2 at Thr 487 by CDK1 promotes dissociation of PRC2 and results in inhibition of its HMTase activity, which in turn derepresses genes silenced by EZH2.

As CDK1 functions as a cell-cycle kinase during G2/M phase, and also phosphorylates EZH2, we next investigated whether CDK1-mediated phosphorylation of EZH2 was regulated during the cell cycle (Fig. 3g, h). In cells with ectopically and endogenously expressed EZH2 phosphorylation of EZH2 at Thr 487 was low in G0/G1 and S phase, but much higher in G2/M phase. This is consistent with the expression level of

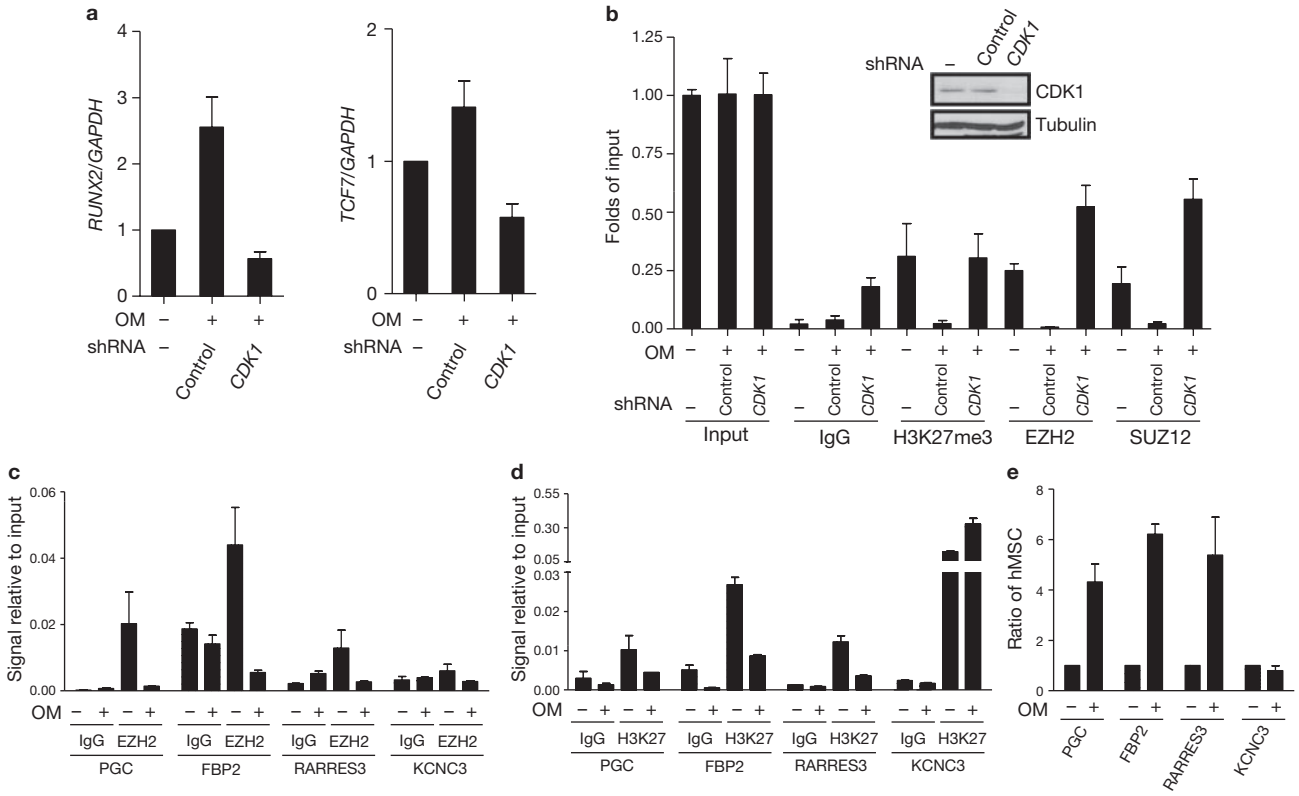

Figure 5 CDK1 regulates EZH2-target gene expression in human mesenchymal stem cells. (**a**) Effect of *CDK1* knockdown on the expression of EZH2-target genes in hMSCs. Cells were cultured in control medium or osteoblast differentiation medium with or without *CDK1* shRNA. mRNA levels of *RUNX2* (left) and *TCF7* (right) were measured by qRT–PCR, and are calculated relative to *GAPDH* expression. Data are means ± s.e.m. ($n = 3$). (**b**) Effect of CDK1 knockdown on the binding of EZH2 to *RUNX2* gene promoter in hMSCs. Cells were cultured in control medium or osteoblast differentiation medium with or without *CDK1* shRNA infection. Quantitative chromatin immunoprecipitation was performed using antibodies against the indicated proteins on the *RUNX2* promoter. Levels of CDK1 are shown by immunoblot (top). (**c**, **d**) Four genes shown to have differential EZH2 binding after osteogenic differentiation from a genome-wide ChIP-on-chip assay were randomly selected for ChIP assay using antibodies against EZH2 (**c**) and H3K27me3 (**d**). hMSCs were cultured in control medium or osteoblast differentiation medium. (**e**) The expression of the four genes analysed in **c** and **d** was assessed by qRT–PCR from hMSCs cultured in control medium or osteoblast differentiation medium.

cyclin B1, which is known to activate CDK1 activity in G2/M phase. We found phosphorylation of EZH2 at Thr 487 occurred during the cell cycle in cells stably expressing wild-type EZH2, but not in cells expressing EZH2^{T487A} (Supplementary Information Fig. S3b). In addition, the expression of several *HOXA* genes was regulated during the cell cycle, with much higher expression level in G2/M phase than in S phase, which correlated with the highest level of EZH2 phosphorylation and the lowest level of H3K27 trimethylation in G2/M phase (Fig. 3i and Supplementary Information Fig. S3b). These results suggest that CDK1 inhibits EZH2 activity and derepresses its target gene expression during cell cycle.

As EZH2 is known to enhance cell proliferation, migration and invasion[4,5,6], and phosphorylation of EZH2 by CDK1 at Thr 487 inhibits EZH2 HMTase activity, we further investigated the effect of the T487A mutation on EZH2-mediated biological functions. Using stable transfectants expressing wild-type EZH2 and EZH2^{T487A}, we did not observe significant differences in cell proliferation (data not shown). However, expression of EZH2^{T487A} significantly enhanced cancer cell migration and invasion (Fig. 3j, k). These results suggest that phosphorylation of EZH2 at Thr 487 by CDK1 inhibits cancer cell migration and invasion.

EZH2 has an important role in regulating stem cell pluripotency and differentiation[12–14]. Human bone-marrow-derived mesenchymal stem cells (hMSCs) are multipotent cells[15]. They differentiate into chondrogenic, adipogenic or osteogenic lineages when cultured under defined *in vitro* conditions[16–18]. hMSCs differentiate into the osteogenic lineage when cultured in osteoblast differentiation medium[19]. However, the mechanisms governing hMSC differentiation are not well understood. Therefore, we investigated whether CDK1 regulation of EZH2 might have a role in hMSC differentiation. Treatment of hMSCs with osteoblast differentiation medium, but not adipocyte differentiation medium, resulted in sustained CDK1 activation (Fig. 4a). The activation of CDK1 was accompanied by an increase of EZH2 phosphorylation at Thr 487 and a decrease of H3K27 trimethylation (Fig. 4a). To determine whether the CDK1–EZH2 pathway is required for osteogenic differentiation, we used *CDK1* shRNAs to knockdown endogenous *CDK1* and measured the effects on hMSC osteogenic differentiation. Continuous incubation of hMSC with osteoblast differentiation medium for 7 days resulted in positive Alizarin Red S staining (a standard marker for osteogenic differentiation; Fig. 4b, B), as well as increased expression of osteogenic marker genes, *RUNX2* and osteopontin (Fig. 4c, lanes 1 and 2), whereas knockdown of *CDK1* by three different shRNAs blocked osteogenic differentiation (Fig. 4b, D–F). The knockdown of *CDK1* by shRNA led to decreased EZH2 phosphorylation, increased H3K27 trimethylation and repression of the osteogenic markers, Runx2 and osteopontin (Fig. 4c, lanes 3 and 4). Similar results were seen in multiple primary cultured hMSCs (Supplementary Information,

Fig. S4a, b and data not shown). Together, the results suggest that the phosphorylation of EZH2 by CDK1 is critical for the osteogenic differentiation of hMSC.

Next, we investigated whether activation of CDK1 by osteogenic differentiation also led to disruption of the PRC2 complex. Indeed, the interaction of EZH2 with SUZ12 and EED was decreased when hMSCs were induced to osteodifferentiation (Fig. 4d). These results support the hypothesis that activation of CDK1 promotes osteogenic differentiation through disruption of the PRC2 complex.

Several genes have been shown to be putative targets of EZH2, such as *RUNX2* and *TCF7*, which are known to be important for osteogenesis[12]. To further investigate whether activation of CDK1 promotes osteogenic differentiation through disruption of the PRC2 complex, we quantified the expression of EZH2-target genes during osteogenesis by qRT–PCR. The expression of *RUNX2* and *TCF7* mRNAs significantly increased during osteogenesis (Fig. 5a). Knockdown of *CDK1* by shRNA significantly inhibited the effect of osteoblast differentiation medium on the increased expression of *RUNX2* and *TCF7* (Fig. 5a). Consistently, a qChIP assay indicated that osteogenic differentiation resulted in decreased binding of EZH2, SUZ12 and H3K27 trimethylation at the promoter of *RUNX2* (Fig. 5b). These changes were reversed with knockdown of *CDK1* by shRNA (Fig. 5b). These results suggest that CDK1 regulates osteogenesis through suppression of methyltransferase activity of EZH2 and promotes derepression of target genes of EZH2 such as osteogenesis-related genes *RUNX2* and *TCF7*.

To further expand our findings, we carried out genome-wide screening to identify EZH2-target genes in hMSCs before and after osteogenic differentiation. We performed ChIP using EZH2 antibody to immunoprecipitate EZH2 and its associated DNA, followed by hybridization with promoter microarrays (ChIP-on-chip). A large number of genes (> 4,000) bind to EZH2, but after osteogenic differentiation less than 30 genes bound (Supplementary Information, Tables S1 and S2), suggesting that EZH2 is disassociated from promoters of its target genes after osteogenic differentiation.

To validate the enrichment profiles of EZH2-target genes, we randomly selected nine EZH2-targeted genes that were bound by EZH2 in hMSC, but lost binding to EZH2 after osteodifferentiation, and quantified for EZH2 and H3K27me3 enrichments in an independent experiment (Supplementary Information, Table S3). In eight of the nine genes the qChIP experiments confirmed the ChIP-on-chip results, with very similar decreased binding of EZH2 (Fig. 5c) and H3K27me3 (Fig. 5d) at these gene promoters after osteogenic differentiation. Consistently, the mRNA expression of these eight genes increased significantly during osteogenesis (Fig. 5e). The data from the three genes that were scored positive, *PGC*, *RARRES3* and *FBP2*, are shown in Figure 5c–e. Similar results were observed for the other five genes (Supplementary Information, Table S3, Fig. S5a, b, c).

In this study, we demonstrated a novel signal pathway in which the protein kinase CDK1 regulates the histone methyltransferase EZH2. We have found that CDK1 phosphorylates EZH2 at Thr 487 thereby disrupting EZH2 binding with SUZ12 and EED, and leading to suppression of H3K27 trimethylation and consequent derepression of target gene expression. This CDK1–EZH2 signalling pathway is important both in cell migration and invasion in cancer cells, and in the regulation of osteogenic differentiation of hMSCs through the modulation of EZH2-targeted osteogenic gene expression.

It is worthwhile to mention that while this manuscript was under revision, an interesting report was published that shows phosphorylation of EZH2 at Thr 350 by CDK1 and CDK2 is important for recruitment of EZH2 and maintenance of H3K27me3 levels at EZH2-target loci[20]. Blockage of Thr 350 phosphorylation not only diminishes the global effect of EZH2 on gene silencing, but also mitigates EZH2-mediated cell proliferation and migration[20]. The impact of EZH2 Thr 350 phosphorylation on H3K27me3 levels in target-gene promoters is not because of changes in stability, formation or intrinsic HMTase activity of PRC2 (ref. 20). In our current study, we have identified a different phosphorylation site of EZH2 by CDK1, Thr 487, which after phosphorylation not only inhibits binding of EZH2 to its targets on the promoter, but also inhibits HMTase activity of EZH2 through disruption of the PRC2 complex. We have further demonstrated that phosphorylation of EZH2 at Thr 487 by CDK1 stimulates mesenchymal stem cell osteogenic differentiation through derepression of putative EZH2-target genes. It is not clear whether a relationship exists between these two phosphorylation sites of EZH2. A systematic study may be required to further investigate the relationship between these two sites. □

METHODS

Methods and any associated references are available in the online version of the paper at http://www.nature.com/naturecellbiology/

Note: Supplementary Information is available on the Nature Cell Biology website

ACKNOWLEDGEMENTS

We thank S. A. Miller and J. Hsu for editorial assistance. We thank A. M. Labaff for characterization of EED antibody. This work was supported by grants from National Institutes of Health (grant R01 CA109311), Kadoorie Charitable Foundations, National Breast Cancer Foundation Inc. and the M. D. Anderson Cancer Center/China Medical University and Hospital Sister Foundation Funds (to M.-C.H), NSC 96-3111-B-039 and NSC 97-3111-B-039 (to M.-C.H., L.-Y.L. and S.-P.Y), NHRI-EX98-9603BC, DOH97-TD-I-111-TM003, DOH98-TD-I-111-TM002 (to L.-Y.L.), DOH97-TD-G-111-041 (to M.-C.H.), DOH99-TD-C-111-005, NSC99-2632-B-039-001-MY3 (to L. –Y.L. and M. –C.H.). In memory of Mrs Serena Lin-Guo for her courageous battle against breast cancer.

AUTHOR CONTRIBUTIONS

M.-C.H., Y.W. and L.-Y.L. designed the project and wrote the paper. M.-C.H. and L.-Y.L. supervised the research. Y.W. performed most of the experiments in Figs 1–3. Y.-H.C. performed mesenchymal stem cell experiments in Figs 4 and 5 and experiments investigating the interaction between EZH2 and CDK1. C.-C.L. performed the mass spectrometry analysis. C.-Y.L. generated and characterized the phospho-EZH2 antibody. S.-P.Y. collected and characterized primary human mesenchymal stem cells. J. L., B.S., C. -C.Y. and J.-Y.Y. assisted with experiments. All authors participated in interpreting the results.

COMPETING FINANCIAL INTERESTS

The authors declare no competing financial interests.

Published online at http://www.nature.com/naturecellbiology
Reprints and permissions information is available online at http://npg.nature.com/reprintsandpermissions/

1. Cao, R. *et al.* Role of histone H3 lysine 27 methylation in Polycomb-group silencing. *Science* **298,** 1039–1043 (2002).
2. Kuzmichev, A., Nishioka, K., Erdjument-Bromage, H., Tempst, P., Reinberg, D. Histone methyltransferase activity associated with a human multiprotein complex containing the Enhancer of Zeste protein. *Genes Dev.* **16,** 2893–2905 (2002).
3. Cao, R., Zhang, Y. The functions of E(Z)/EZH2-mediated methylation of lysine 27 in histone H3. *Curr. Opin. Genet. Dev.* **14,** 155–164 (2004).
4. Varambally, S. *et al.* The polycomb group protein EZH2 is involved in progression of prostate cancer. *Nature* **419,** 624–629 (2002).
5. Kleer, C. G. *et al.* EZH2 is a marker of aggressive breast cancer and promotes neoplastic transformation of breast epithelial cells. *Proc. Natl Acad. Sci. USA* **100,** 11606–11611 (2003).
6. Bracken, A. P. *et al.* EZH2 is downstream of the pRB-E2F pathway, essential for proliferation and amplified in cancer. *EMBO J.* **22,** 5323–5335 (2003).

7. Bachmann, I. M. *et al.* EZH2 expression is associated with high proliferation rate and aggressive tumor subgroups in cutaneous melanoma and cancers of the endometrium, prostate, and breast. *J. Clin. Oncol.* **24,** 268–273 (2006).
8. Gonzalez, M. E. *et al.* Downregulation of EZH2 decreases growth of estrogen receptor-negative invasive breast carcinoma and requires BRCA1. *Oncogene* **28,** 843–853 (2009).
9. Van Hoof, D. *et al.* Unraveling the human embryonic stem cell phosphoproteome. *Cell Stem Cell* **5,** 214–226 (2009).
10. Imbach, P. *et al.* 2, 6, 9-trisubstituted purines: optimization towards highly potent and selective CDK1 inhibitors. *Bioorg. Med. Chem. Lett.* **9,** 91–96 (1999).
11. van den Heuvel, S. and Harlow, E. Distinct roles for cyclin-dependent kinases in cell cycle control. *Science* **262,** 2050–2054 (1993).
12. Bracken, A. P. *et al.* Genome-wide mapping of Polycomb target genes unravels their roles in cell fate transitions. *Genes Dev.* **20,** 1123–1136 (2006).
13. Boyer, L. A. *et al.* Polycomb complexes repress developmental regulators in murine embryonic stem cells. *Nature* **441,** 349–353 (2006).
14. Lee, T. I. *et al.* Control of developmental regulators by Polycomb in human embryonic stem cells. *Cell* **125,** 301–313 (2006).
15. Barry, F. P. & Murphy, J. M. Mesenchymal stem cells: clinical applications and biological characterization. *Int. J. Biochem. Cell Biol.* **36,** 568–584 (2004).
16. Bruder, S. P. *et al.* Mesenchymal stem cells in bone development, bone repair and skeletal regeneration therapy. *J. Cell Biochem.* **56,** 283–294 (1994).
17. Mackay, A. M. *et al.* Chondrogenic differentiation of cultured human mesenchymal stem cells from marrow. *Tissue Eng.* **4,** 415–428 (1998).
18. Pittenger, M. F. *et al.* Multilineage potential of adult human mesenchymal stem cells. *Science* **284,** 143–147 (1999).
19. Jaiswal, N., Haynesworth, SE., Caplan, A. I. and Bruder, S. P. Osteogenic differentiation of purified, culture-expanded human mesenchymal stem cells *in vitro*. *J. Cell. Biochem.* **64,** 295–312 (1997).
20. Chen, S. *et al.* Cyclin-dependent kinases regulate epigenetic gene silencing through phosphorylation of EZH2. *Nat. Cell Biol.* **12,** 1108–1114 (2010).

METHODS

Cell lines. Breast cancer cell lines (MCF-7, SKBr3, MDA-MB435, and MDA-MB468); human embryonic kidney cell line (293 and 293T); and human cervical cancer cell line (HeLa) were obtained from American Type Culture Collection (Manassas). The cells were grown on tissue culture dishes in a 1:1 (v/v) mixture of Dulbecco's modified Eagle's minimum essential medium and Ham's F12 medium (DMEM/F12) supplemented with 10% of heat-inactivated fetal bovine serum (FBS). Human MSC cell line was cultured in low glucose DMEM containing 10% FBS. Osteoblast differentiation was induced with low glucose DMEM containing 10% FBS, 10 nM dexamethasone, 50 μg ml^{-1} ascorbic acid-2 phosphate, and 10 mM β-glycerophosphate. For adipocyte differentiation, hMSCs were cultured in low glucose DMEM with 10% FBS supplemented with 100 nM dexamethasone, 50 μg ml^{-1} ascorbic acid-2 phosphate, 50 μM indomethacin, 10 μg ml^{-1} insulin, and 0.45 μm 3-isobutyl-1-methylxanthine. The differentiation medium was replaced every 3 days during differentiation period.

Antibodies. Antibodies to c-Myc (1:3,000), haemagglutinin (1:3,000; Roche Molecular Biochemicals), trimethyl-H3K27 (1:10,000), EED (1:3,000; Upstate), SUZ12 (1:2,000), phospho-CDK1 (Thr161; 1:1,000; Cell Signaling), CDK1 (1:1,000), Runx2 (1:1,000), Osteopontin (1:1,000; Santa Cruz Biotechnology) and EZH2 (1:2,000; BD Biosciences) were purchased. Mouse antiserum against the phosphorylation site of EZH2 at Thr 487 were produced with a synthetic phosphopeptide: EDVD(pT)PPRKKKRKH.

CGP74514A treatment. CDK1 inhibitor CGP7451A was obtained from Sigma (Cat # C3353). Cell lines were treated with CGP74514A (2 μM) for 16 h.

Identification of phosphorylation sites by mass spectrometry. To identify *in vivo* phosphorylation site of EZH2, lysates of HeLa cells were immunoprecipitated with anti-EZH2. *In vitro* phosphorylation site of EZH2 was identified by *in vitro* kinase assay using recombinant cyclin B, CDK1 and full-length GST–EZH2. After protein gel electrophoresis, bands were excised from gels, and subjected to tryptic digestion. After being isolated by immobilized metal affinity chromatography, the enriched phosphopeptides were analysed by micro-liquid chromatography/tandem mass spectrometry (LC–MS/MS) by using an Ultimate capillary LC system (LC Packings) coupled to a QSTARXL quadrupole (Q)–time-of-flight (TOF) mass spectrometer (Applied Biosystems). The product ion spectra generated by nanoscale capillary LC-MS/MS were searched against National Center for Biotechnology Information databases for exact matches using the ProID (Applied Biosystems) and MASCOT search programs. Carbamidomethyl cysteine was set as a fixed modification, and serine, threonine and tyrosine phosphorylation were set as variable modifications. All phosphopeptides identified were confirmed by manual interpretation of the spectra.

GST pulldown assays. GST and GST–EZH2 protein (10 μg) were incubated at 4 °C with 2 mg HeLa cell-extract overnight, and the GST-tagged proteins were recovered by incubating the reaction at 4 °C for 3 h with 20 μl glutathione–Sepharose 4B beads. The bead pellet was washed three times with 1 ml buffer (20 mM Tris–HCl at pH 7.5, 150 mM NaCl, 10% glycerol, 1% Triton X-100 and 2 mM EDTA). Boiled samples were then subjected to SDS–PAGE.

Plasmids. DNA plasmids encoding CDK1–HA (Addgene plasmid 1888), CDK1-DN–HA (Addgene plasmid 1889), Rc/CMV cyclin B2 (Addgene plasmid 10911) were from Addgene. Dominant-negative mutant CDK1 (DN-CDK1) is a D146N mutant[11]. pcDNA3-His-Myc–EZH2 was a gift from A. Chinnaiyan. Site-directed mutagenesis was performed according to the manufacturer's protocol (Clontech; Palo Alto, CA). Thr 487 in EZH2 was replaced with alanine, using the primer: T487A, 5′-GAGGATGTGGATGCTCCTCCAAGGAAAAAG-3′. To generate constructs for bacterial expression of wild-type and mutant EZH2 tagged with glutathione-*S*-transferase (GST), DNA fragments encoding full-length EZH2 were subcloned into the bacterial expression vector pGEX6P-1 (Amersham Biosciences). Wild-type and mutant EZH2 proteins were inducibly expressed in *Escherichia coli* strain BL21 and purified by glutathione–Sepharose chromatography (Amersham Biosciences).

RNAi plasmid. RNA interference was performed using lentiviral short hairpin RNA (shRNA) libraries[21]. MISSION™ TRC-Hs (Human) shRNA Library were bought from research institute Academia Sinica in Taiwan.

Primers for *CDK1* shRNA were: shRNA-CDK1-A01 (Clone ID TRCN0000000582): 5′-CCGGGCTGTACTTCGTCTTCTAATTCTCGAGAA-TTAGAAGACGAAGTACAGCTTTTT-3′; shRNA-CDK1-B01 (Clone ID TRCN0000000583): 5′-CCGGGTGGAATCTTTACAGGACTATCTCGAG-ATAGTCCTGTAAAGATTCCACTTTTT-3′ and shRNA-CDK1-D01 (Clone ID TRCN0000000585): 5′-CCGGTGGCTTGGATTTGCTCTCGAACTCGAG-TTCGAGAGCAAATCCAAGCCATTTTT-3′.

Quantitative real-time RT–PCR. Total RNA was extracted from cells. Quantitative RT–PCR (qRT–PCR) was performed using SYBR Green dye on a Bio-Rad PCR machine. Briefly, 1 μg of total RNA was reverse transcribed into cDNA using SuperScript III (Invitrogen) in the presence of random hexamers. All reactions were performed in triplicate with SYBR Green Master Mix (Applied Biosystems) plus 1 μM of both the forward and reverse primer according to the manufacturer's recommended thermocycling conditions, and then subjected to melt-curve analysis. The calculated quantity of the target gene for each sample was divided by the average sample quantity of the housekeeping genes, glyceraldehyde-3-phosphate dehydrogenase (*GAPDH*) to obtain the relative gene expression. The primer sequences for the transcript analysed are provided in Supplementary Information, Table S4.

Chromatin immunoprecipitation (ChIP) assays. The ChIP assay was carried out with antibodies against trimethyl-H3K27 (Rabbit polyclonal from Upstate; 07-449), SUZ12 (Rabbit polyclonal from Upstate; 07-379) and C-Myc (Roche Molecular Biochemicals). The assay was performed using the EZ-ChIP kit (Millipore) according to the manufacturer's instructions. The cells were cross-linked for 10 min by addition of formaldehyde to a final concentration of 1%. The cross-linking was stopped by adding 1/20 volume of 2.5 M glycine. This was followed by cell lysis and sonication. Antibody incubations were carried out overnight at 4 °C. Reversal of cross-linking was carried out at 65 °C for 3 h. The purified DNA was analysed by quantitative PCR. The primer sequences for the promoters analysed are provided in Supplementary Information, Table S4.

Immunoprecipitation and immunoblotting. Cells were washed twice with PBS and scraped into 500 μl of lysis buffer. After brief sonication, the lysate was centrifuged at 14,000*g* for 10 min at 4 °C to remove insoluble cell debris. Immunoprecipitation and immunoblotting were performed as described[22].

***In vitro* kinase assay.** Recombinant cyclin B and CDK1 (New England Biolabs) were incubated with 1 μg of purified GST–EZH2 (wild-type or mutant) in the presence of 5 μCi of [γ-^{32}P]ATP and 50 μM cold ATP in kinase buffer for 30 min at 30 °C. Alternatively, cells expressing CDK1 (and treated with *CDK1* shRNA) were labelled with 0.2 mCi ml^{-1} [^{32}P]-orthophosphate for 3 h (Fig. 2g). Reaction products were resolved by SDS–PAGE, and ^{32}P-labelled proteins were visualized by autoradiography.

***In vitro* histone methyltransferase assay.** MCF7 cells stably expressing Myc-His-tagged wild-type EZH2 and EZH2^{T487A} mutant were lysed, and tagged proteins were purified by using a combination of protein G-crosslinked Myc antibody and nickel column purification. The *in vitro* HMTase assay was performed as described[23], except for slight modifications. Briefly, 30 μl of reaction mixture containing the nickel beads attached to the purified protein, 2 μg of oligonucleosome as substrates, and 2 μCi of *S*-adenosyl-L-(methyl-^{3}H) methionine (SAM; Amersham Biosciences) as the methyl donor in methylase activity buffer (50 mM Tris-HCl at pH 8.5, 100 mM NaCl and 10 mM dithiothreitol; DTT) was incubated for 1 h at 30 °C. Proteins were resolved by 15% SDS–PAGE gel and visualized by Coomassie-blue staining and autoradiography.

ChIP-on-chip assay for EZH2. hMSCs were differentiated into osteoblasts and then cells were harvested for the ChIP-on-chip assay using NimbleGen Human ChIP 385K promoter array Two-set. The procedure was performed according to manufacturer's instructions (NimbelGen company).

Cell migration assay. Migration assays were performed in Transwell filter inserts in 24-well tissue culture plates (BD Bioscience). The polycarbonate membrane filters of Transwell contain pores 8 μm in diameter. Cells were detached at 90% confluence, washed once in PBS, and resuspended in serum-free Dulbecco's Modified Eagle Medium (DMEM). Cell suspension (250 μl) was added to inserts

DOI: 10.1038/ncb2139

at a density of 1×10^5 cells per insert. DMEM containing 10% (v/v) fetal calf serum (FCS) was added to the lower wells. Migration was allowed to proceed at 37 °C for 16 h. Cells that did not migrate through the filters were removed using cotton swabs, and cells that migrated through the inserts were fixed and stained with crystal violet. The number of migrated cells per microscopic field (at original magnification ×200) was counted visually under a light microscope. The data were expressed as the average number of cells from five randomly selected fields. Data from three independent experiments were pooled and analysed using a two-tailed, Student's *t*-test.

Cell invasion assay. Invasion was measured using Biocoat Matrigel invasion chambers (BD Biosciences) by following the manufacturer's protocol. Briefly, cells at the 90% confluent stage were detached. DMEM containing 10% FCS was placed in the lower well, and 1×10^5 cells in 250 μl of serum-free medium were loaded to the upper chamber of the Matrigel-coated insert and incubated at 37 °C for 40 h. Cells that invaded to the lower surface of the filter were fixed and stained with crystal violet and quantified with light microscope at original magnification ×200. The data were expressed as the average number of cells from five randomly selected fields and analysed statistically using a two-tailed, Student's *t*-test. The experiments were repeated three times.

21. Moffat, J. *et al.* A lentiviral RNAi library for human and mouse genes applied to an arrayed viral high-content screen. *Cell* **124,** 1283–1298 (2006).
22. Lee, D. F. *et al.* IKKβ suppression of TSC1 links inflammation and tumor angiogenesis via the mTOR pathway. *Cell* **130,** 440–455 (2007).
23. Wang, H. *et al.* Methylation of histone H4 at arginine 3 facilitating transcriptional activation by nuclear hormone receptor. *Science* **293,** 853–857 (2001).

nature cell biology

DOI: 10.1038/ncb2139

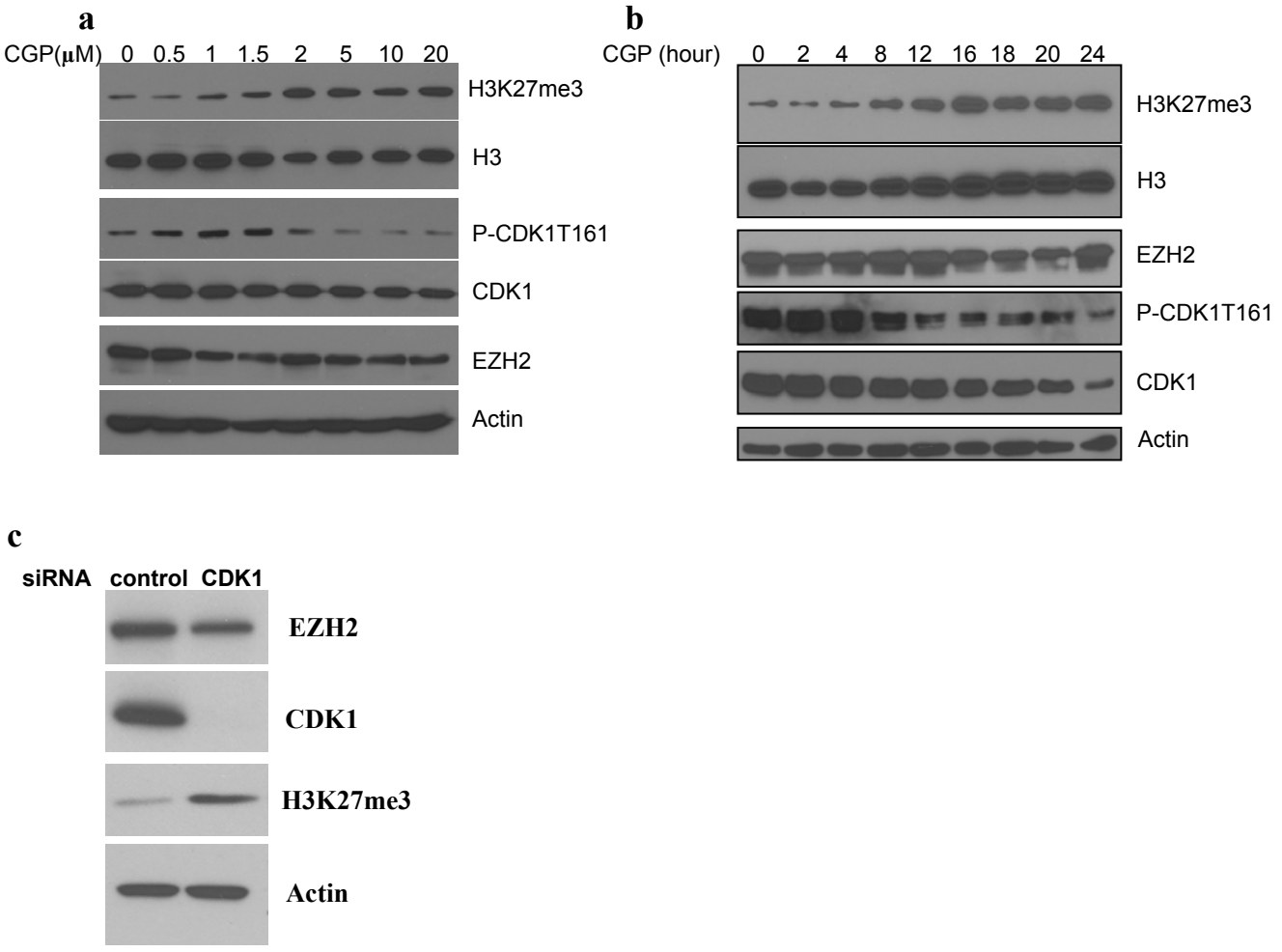

Figure S1 Inhibition of CDK1 enhances H3K27 trimethylation. (a)H3K27 trimethylation increased by the treatment of CGP in a dose depedent manner. Cells were treated with CGP for different concentrations, and H3K27 trimethylation was measured by Western blotting. **(b)** H3K27 trimethylation is dynamically regulated by CDK1. Cells were treated with 5 μM CGP for different times, and H3K27 trimethylation was measured by Western blotting. **(c)** Knock-down of CDK1 enhances H3K27 trimethylation. Western blotting analysis of H3K27 trimethylation in HeLa cells transfected with control or CDK1 SMARTpool siRNA (Dharmacon RNA Technologies) for 48 hrs.

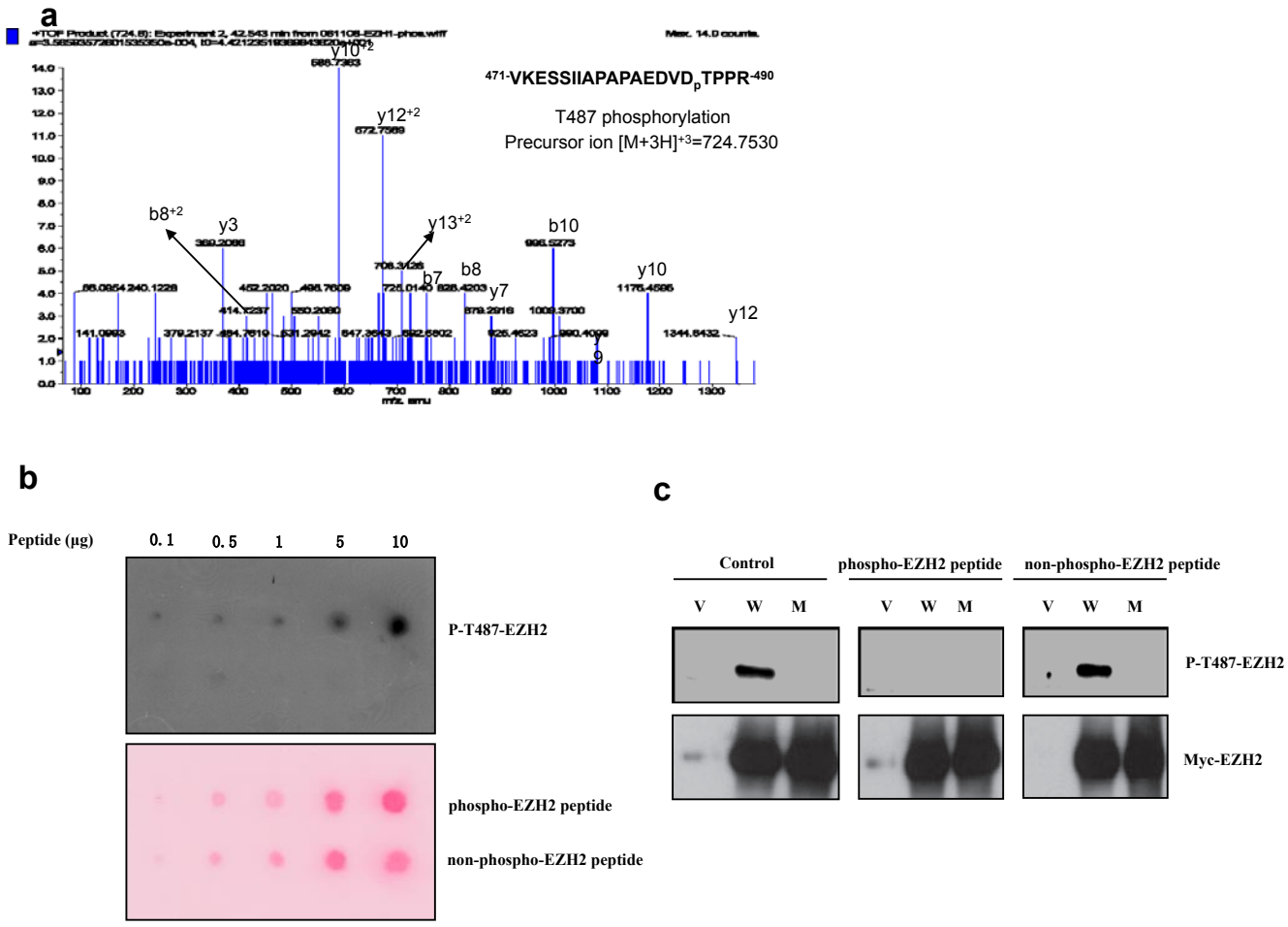

Figure S2 CDK1 phosphorylated EZH2 at Thr487 *in vivo*. **(a)**Lysates of Hela cells were immunoprecipitated with anti-EZH2 and analyzed by mass spectrometry analysis. **(b)** Dot blot assay of the EZH2 peptides containing phosphorylated or non-phosphorylated Thr487. Phospho- or non-phospho-peptides were immunoblotted with an phosphoT487-EZH2 antibody. **(c)** Lysates of 293 cells transfected with Myc-EZH2 or Myc-T487A-EZH2 mutant were immunoprecipitated with anti-Myc. Anti-phosphoT487-EZH2 sera were pre-incubated with peptide (50 mg/mL) at 37 oC for 30 min then immunoblotted. Membrane was stripped and re-immunoblotted with anti-myc antibody. V, Vector; W, WT-EZH2; M, T487A-EZH2 mutant.

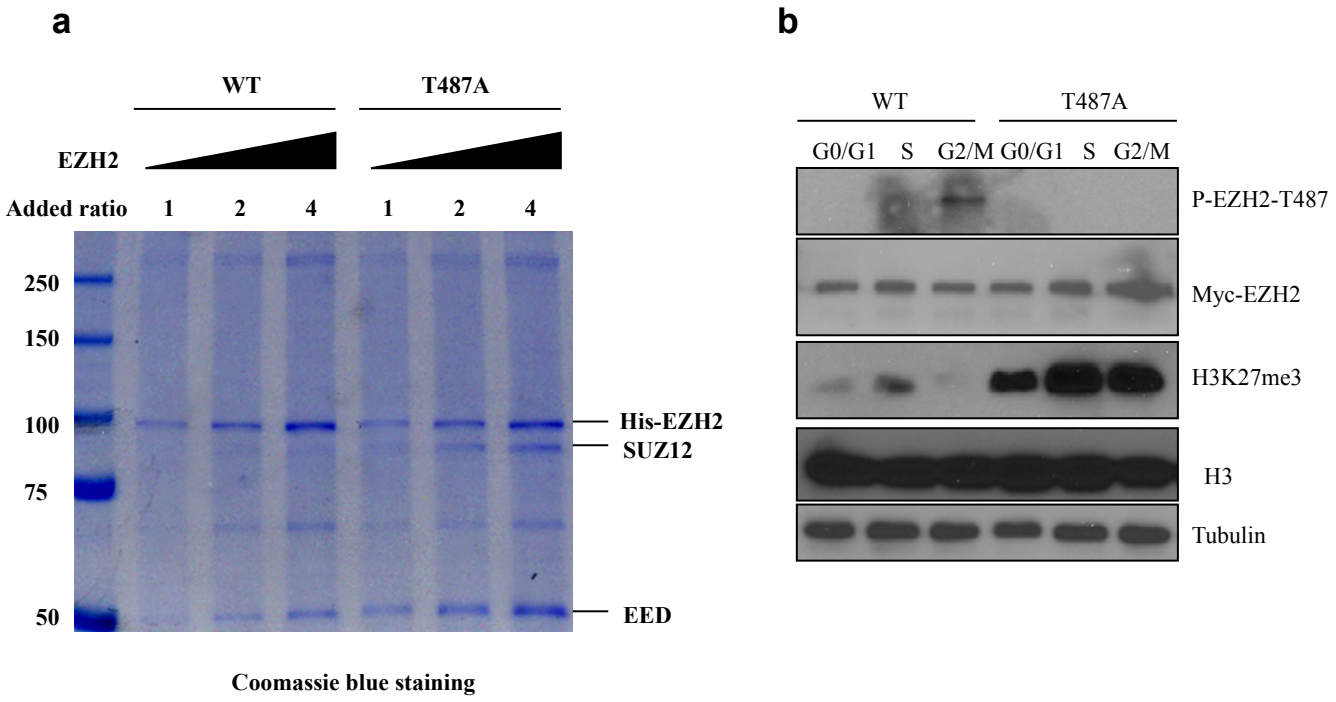

Figure S3 (a) Phosphorylation of EZH2 at Thr 487 disrupts binding of EZH3 with SUZ12 and EED. PRC2 complex were purified from MCF7 cell lines stably expressing Myc-His-tagged WTEZH2 or T487A-EZH2 mutant by using a combination of protein G-crosslinked Myc antibody and nickel column purification. PRC2 complex from WT-EZH2 or T487A-EZH2 mutant were titrated, 0.5, 1, and 2 μg proteins were loaded on SDS-PAGE gel, then stained by coomassie blue. Left side showed the molecular weight marker. Right side showed the names of subunit of the PRC2 complex. **(b)** Phosphorylation of EZH2 at Thr487 was regulated during cell cycle. MCF7 cell lines stably expressing WT-EZH2 or T487A-EZH2 mutant were treated either by serum starvation (to collect cells at G0/G1 phase) or by double thymidine blockage and release to collect cells at S and G2/M phases. Then cells lysates were immunoblotted with antibodies as shown.

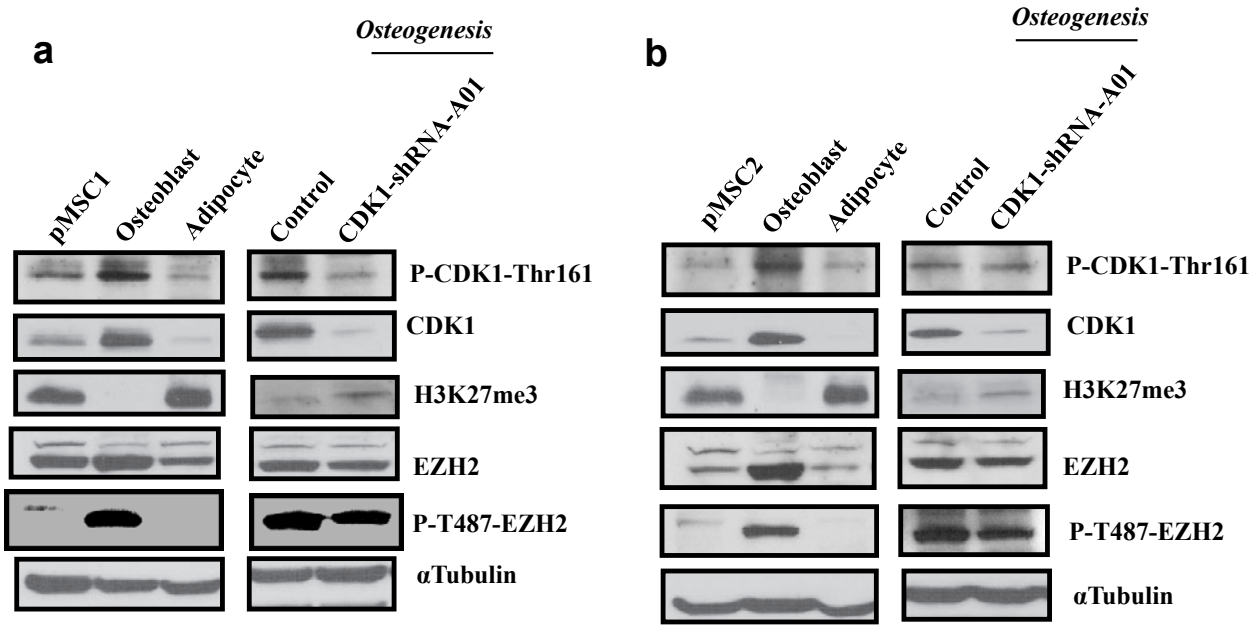

Figure S4 Osteoblast differentiation medium induces activation of CDK1 and phosphorylation of EZH2 in primary hMSC. **(a)** and **(b)** The primary hMSC (pMSC1 and pMSC2) were cultured in control medium or OM with or without CDK1 shRNA infection. Lysates were subjected to immunoblot analysis using antibodies as shown.

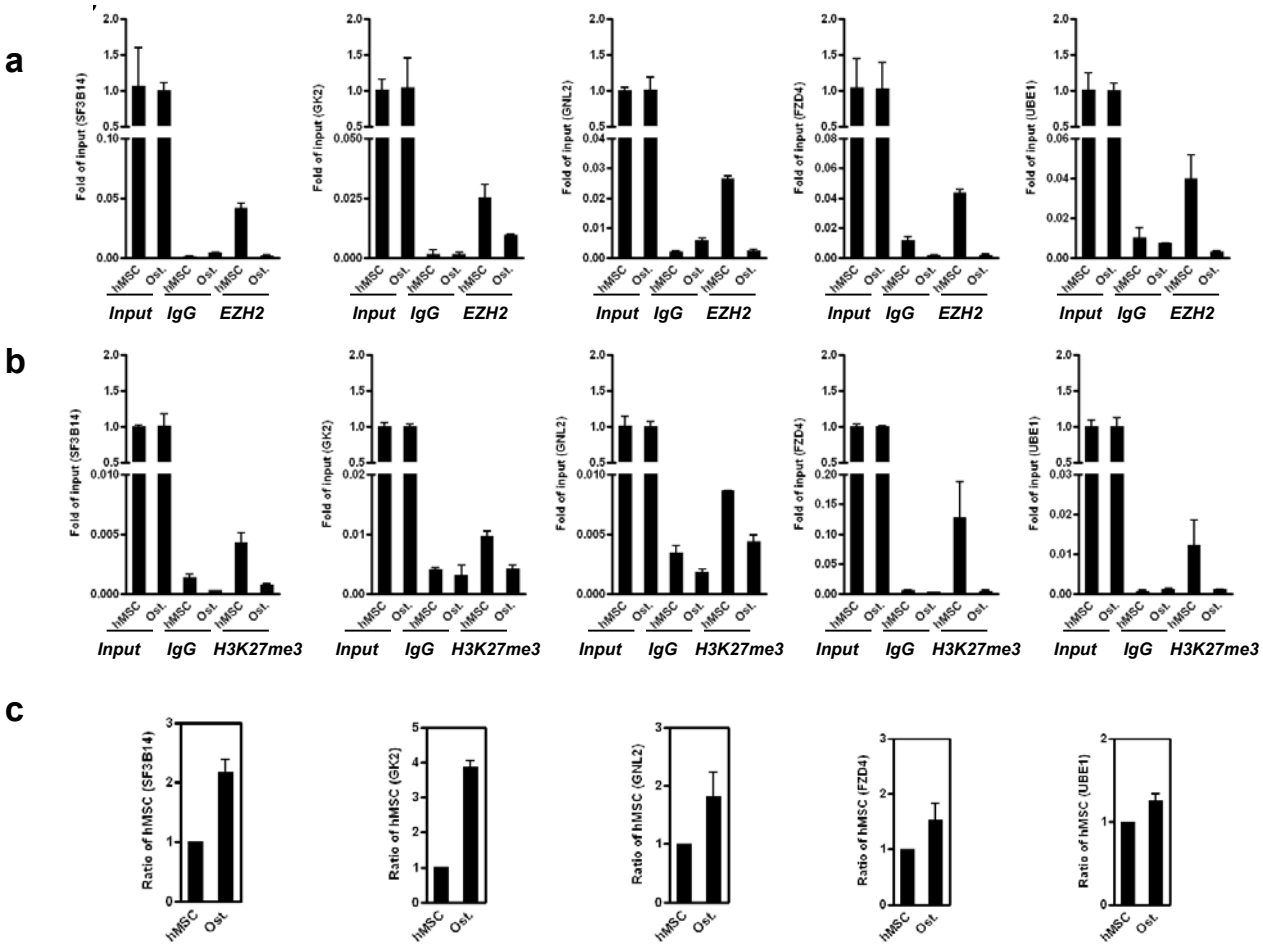

Figure S5 Validation of ChIP-on-chip results for five genes. These five genes were randomly selected from ChIP-on-chip results whose binding to EZH2 were lost after osteogenic differentiation. qChIP were done on the promoters of the five genes indicated by using (**a**)EZH2 antibody and (**b**) H3K27me3 antibody. **(c)** qRT-PCR detection of the expression of the five genes.

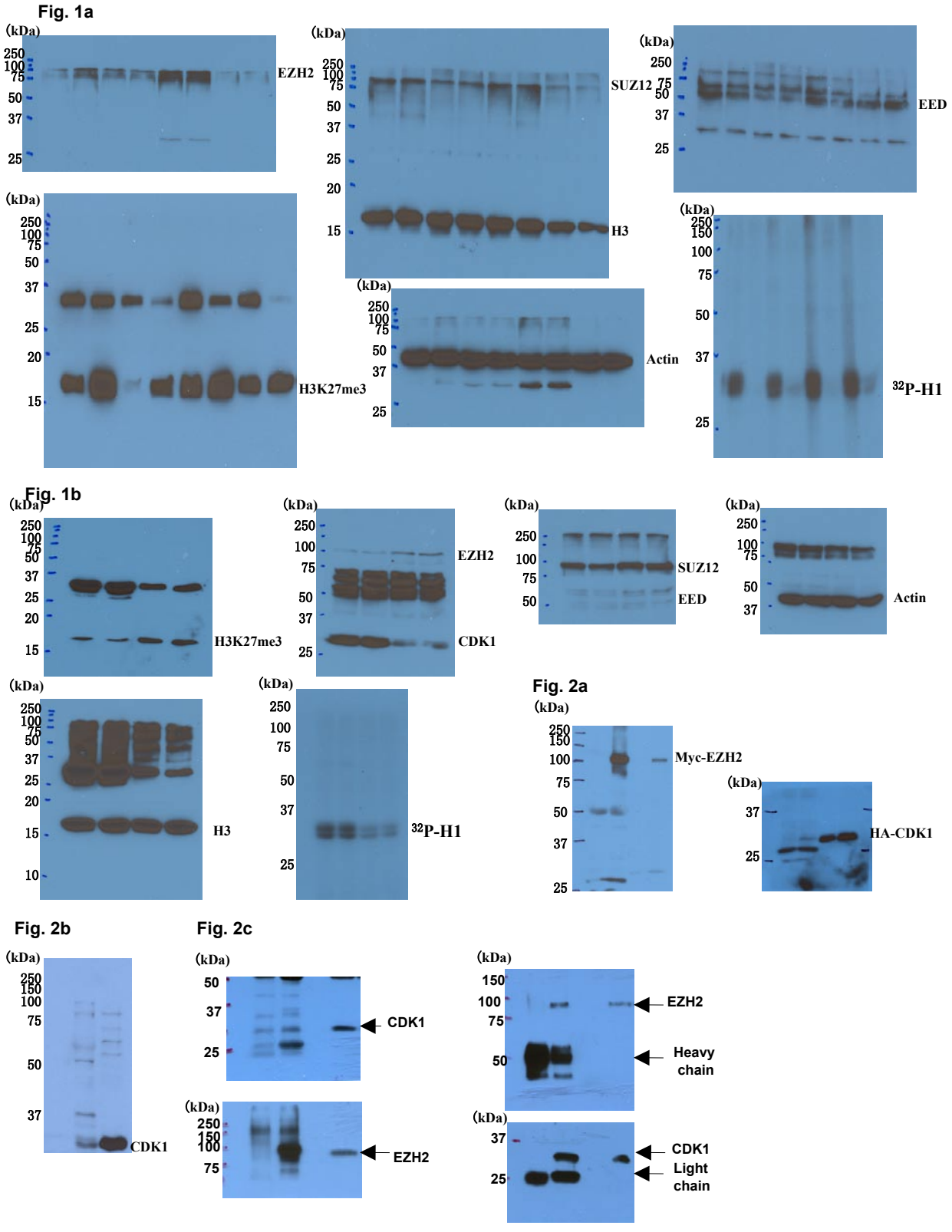

Figure S6 Full scans

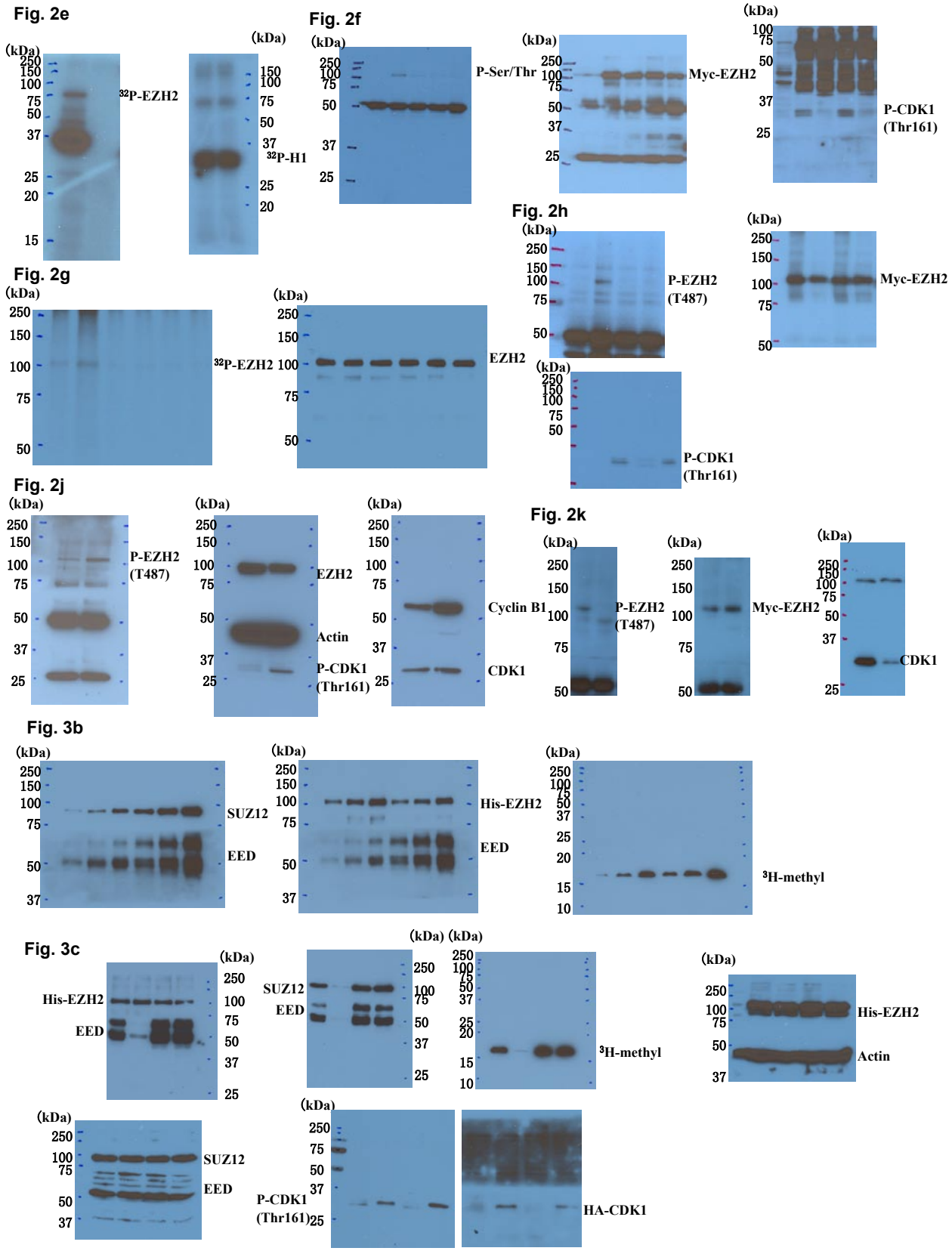

Figure S6 Full scans continued

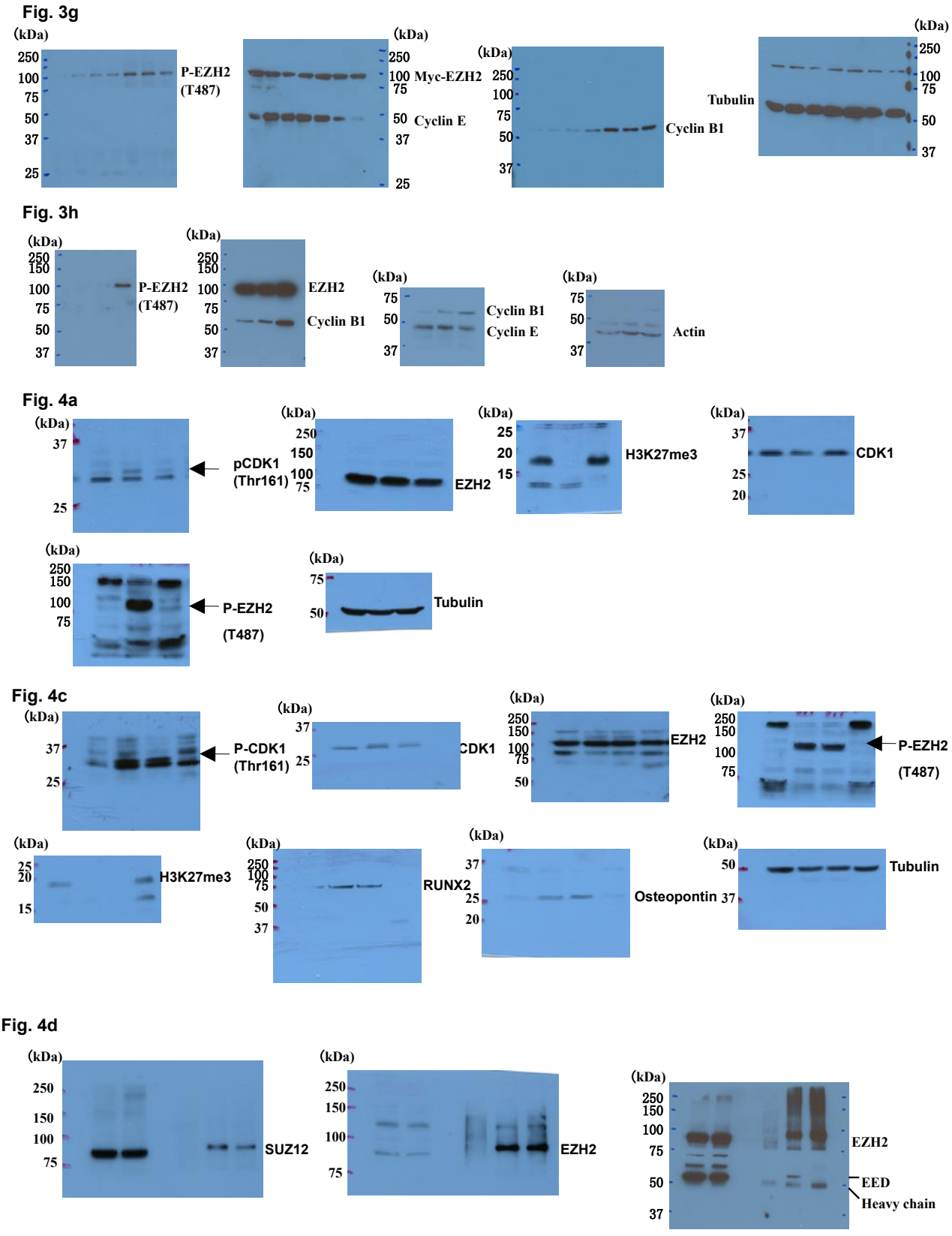

Figure S6 Full scans continued